Highlights

Automatic Processing of Dynamic Responses Via Wavelet Transform for the Development of Dynamic Equivalent Models

Efthimios P. Saroudis,Theofilos A. Papadopoulos,Georgios A. Barzegkar-Ntovom,Eleftherios O. Kontis,Nikolaos Mitianoudis,Grigoris K. Papagiannis

- Wavelet transform based signal processing for dynamic equivalencing
- Event-detection and filtering procedures
- Investigations with synthetic signals, simulated responses and measured data
- Systematic evaluation with other filtering techniques
- Gaussian and long tail noise distributions are examined

Automatic Processing of Dynamic Responses Via Wavelet Transform for the Development of Dynamic Equivalent Models⋆

Efthimios P. Saroudis[a], Theofilos A. Papadopoulos[a,*], Georgios A. Barzegkar-Ntovom[b], Eleftherios O. Kontis[c], Nikolaos Mitianoudis[a] and Grigoris K. Papagiannis[b]

[a]Department of Electrical and Computer Engineering, Democritus University of Thrace, Xanthi, Greece
[b]Power Systems Laboratory, School of Electrical and Computer Engineering, Aristotle University of Thessaloniki, Thessaloniki, Greece
[c]Department of Electrical and Computer Engineering, University of Thessaly, Volos, Greece

ARTICLE INFO

Keywords:
Dynamic Equivalencing
Event detection
Filtering
Noise distributions
Power system dynamics
Wavelet transform

ABSTRACT

The ever-increasing requirements for electricity, the emergence of microgrids and the escalating penetration of distributed generators has reinvigorated the interest in dynamic equivalencing of distribution networks, due to its significance in power system analysis. Scope of this paper is to propose an efficient method for event detection and filtering of dynamic responses based on the wavelet transform (WT), in order to improve the quality of signals used for the derivation of dynamic equivalent models. The accuracy of the proposed method is tested using artificially created noisy responses, by applying Gaussian, Laplace, and Student's-t noise distributions. Comparisons with other filtering techniques are also performed and the impact of all methods on the derivation of accurate equivalent model parameters is quantified and analyzed. The performance of the proposed method is also evaluated by using RMS responses obtained from a large-scale distribution network model as well as by analysing laboratory measurements; results verify the efficiency and applicability of the WT-based processing procedure, by achieving a parameter estimation error well below 1%. It is noteworthy that the average computational burden throughout the process remains under 0.39 s.

1. Introduction

The importance of accurate modelling of distribution networks (DNs) has been demonstrated in numerous studies in the literature, such as transient stability, small disturbance and load flow analyses [1]. Typically, to perform stability studies, power system operators represent DNs and main power system loads using reduced order equivalents [2, 3]. Traditionally, this was imposed by the limited performance of computational systems that prohibited the use of detailed models for the representation of all power system components. Nowadays, despite the progress in computing systems, the need for data confidentiality still imposes the use of reduced-order models [4]. Additionally, the advent of distributed renewable energy resources (DRESs) and the transformation of DNs to active components, i.e., to active distribution networks (ADNs), poses several challenges and obstacles for the development and maintenance of detailed models [4, 5]. Therefore, during the last years several research efforts have been devoted to the development of reduced-order equivalents for the modeling and analysis of new types of loads and ADNs [4, 5, 6, 7].

The main challenge in ADN dynamic equivalencing lies in determining an appropriate equivalent model structure and accurately identifying the parameters that represent the characteristics of various types of loads and DRESs connected to it [8]. Generally, regardless of the chosen model structure, the main approaches to develop equivalents are categorized into component- and measurement- based [2]. The former is a bottom-up approach, that requires detailed knowledge and data of network components, which are difficult, if not impossible, to be determined [6]. In this sense, despite its distinct advantages, the component-based approach cannot be easily implemented to develop equivalent models for extended ADNs that host several types of DRESs and modern loads. On the other hand, the measurement-based approach is a top-down methodology that relies on field measurements recorded at indicative substations, e.g., point of interconnection of ADNs, during system disturbances. In this approach, model parameters are identified by applying optimization and/or system identification techniques [9]. The main advantage of this method lies in the fact that the dynamic behavior of the examined system is directly reflected in the modelling process [10]. Nowadays, the application of the measurement-based approach is essentially favored due to the advent of smart grid technologies and the maturing of data capturing systems, e.g., phasor measurement units (PMU) [11], [12].

Nevertheless, the efficacy of the measurement-based approach highly depends on the quality of the measured signals [9], [13], [14]. Therefore, to enhance the performance of the derived models, a series of tasks must be performed prior

⋆The research work was supported by the Hellenic Foundation for Research and Innovation (H.F.R.I.), Greece under the "First Call for H.F.R.I. Research Projects to support Faculty members and Researchers and the procurement of high cost research equipment grant" (Project No: HFRI-FM17-229)

*Corresponding author
evthsaro1@ee.duth.gr (E.P. Saroudis); thpapad@ee.duth.gr (T.A. Papadopoulos); gbarzegk@ee.duth.gr (G.A. Barzegkar-Ntovom); elkontis@uth.gr (E.O. Kontis); nmitiano@ee.duth.gr (N. Mitianoudis); gpapagia@ece.auth.gr (G.K. Papagiannis)
ORCID(s): 0000-0001-5990-4934 (E.P. Saroudis); 0000-0001-6384-1964 (T.A. Papadopoulos); 0000-0001-9192-4337 (G.A. Barzegkar-Ntovom); 0000-0001-7595-9038 (E.O. Kontis); 0000-0003-0898-6102 (N. Mitianoudis); 0000-0002-9470-8573 (G.K. Papagiannis)

to the parameter estimation procedure. These tasks mainly include: i) event detection, i.e., detection of the exact time the examined event occurred, and ii) data processing to improve the quality of the measured responses by reconstructing the signal in case of missing data and filtering measurement noise, outliers and ambient noise [13]. Missing data may occur as a result of temporary communication or measurement equipment failure. They are usually detectable and can be recovered via interpolation techniques [13], [15]. Outliers are observations/recordings that deviate significantly from normal measurements [16]. Outliers and measurement noise are induced by recording systems, communication channels, instruments, etc. [17]. Ambient noise is inherent in the data and is the result of small perturbations caused by the random varying behavior of loads and generation [12]. This ambient noise is usually referred as ambient data and is assumed to be relatively statistically stationary [18].

Despite the recognized need for further research in measurement processing, as underlined in [7] and [19], and its proven significance in improving the accuracy of developed equivalent models, only a limited number of papers deal with data processing techniques [13]. In this context, in order to facilitate the development of measurement-based equivalent models, a methodology is formulated in this paper for the automatic processing of dynamic responses. The proposed methodology is based on the wavelet transform (WT), which constitutes an efficient mathematical tool for the analysis of measured data with nonstationary characteristics. The proposed methodology aims on the online detection of dynamic disturbances that are suitable for the development of equivalent models and on the filtering of the measured data. A preliminary version of the developed methodology is presented in [20], aiming on the derivation of first-order dynamic load models. In this paper, the work of [20] is extended by: i) testing the proposed method for the analysis of more complex power system dynamic phenomena, e.g., oscillatory responses, ii) developing dynamic equivalent models for conventional DNs that host induction motors (IM) as well as for ADNs with high penetration levels of DRESs, iii) verifying the applicability of the proposed methodology using measurements acquired from a laboratory scale ADN. The performance of the proposed method is validated by means of: i) synthetic signals, distorted by different noise distributions, ii) dynamic responses obtained from RMS simulations conducted using the PowerFactory - DIgSILENT software [21], and iii) laboratory measurements. The proposed method is also compared with other filtering techniques, namely low-pass filtering (LPF), moving average (MA), and Savitzky-Golay (SG), in terms of the quality of the filtered responses and the accuracy of the identified parameters.

The rest of the paper is organized as follows: In Section 2 the theoretical background of the WT is presented. The proposed methodology is formulated in Section 3, and in Section 4 different noise distributions are discussed. In Section 5 the validation of the proposed method by means of synthetic signals is performed. In Section 6, the proposed method is used to derive equivalent models for conventional DNs and ADNs. Evaluation using laboratory measurements is conducted in Section 7. Finally, Section 8 summarizes the main findings and concludes the paper.

2. Wavelet Analysis

The WT is a sophisticated frequency analysis technique widely used for feature detection, noise removal and other signal processing applications [11, 22, 23]. Wavelets are a class of functions that decompose signals into time-varying frequency components and present accurate time–frequency localization and efficient adaptivity to local signal features. There are several WT basis function families $\Psi[n]$, known as mother (prototype) wavelets, with one of the most known being the Daubechies (db$x$). Note that x stands for the order of the Daubechies wavelet [24]. To construct an orthogonal basis, dyadic translations and dilations of the discrete WT (DWT) are applied to the mother wavelet function by means of (1) [25]:

$$\Psi_{(s,\,l)}[n] = 2^{-s/2} \cdot \Psi[2^{-s}n - l] \tag{1}$$

where the scale index s indicates the wavelet width and the location index l gives its translation. Effectively, the DWT is a band-pass filter with a scaling factor of powers of two in the time domain; thus, it halves the bandwidth at every subsequent level of the DWT.

More explicitly, a discrete signal $f[k]$, $k = 0, \ldots, K-1$, is decomposed in terms of a high-pass filter (HPF) $h[k]$ and a low-pass filter (LPF) $g[k]$ into high-frequency and low-frequency components, i.e., the detail $cD[k]$ and approximation $cA[k]$ coefficients, respectively [25], [26], defined as [27]:

$$cD[k] = \sum_{n=-\infty}^{\infty} f[n] \cdot h[2k - n] \tag{2}$$

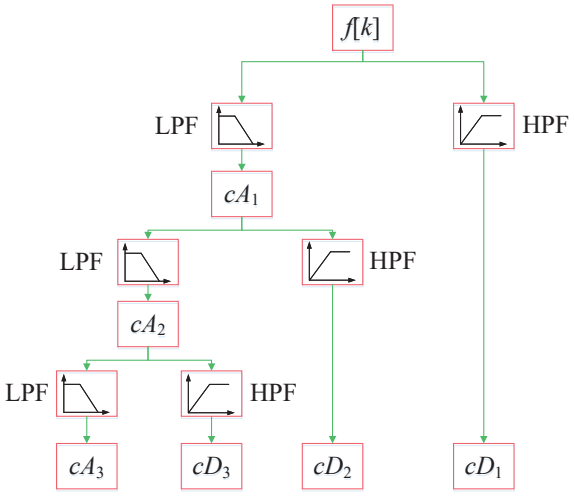

Figure 1: Example of three-level WT decomposition.

$$cA[k] = \sum_{n=-\infty}^{\infty} f[n] \cdot g[2k - n] \tag{3}$$

Filter $g[k]$ is a quadrature mirror filter of $h[k]$ in terms of:

$$g[k] = (-1)^k \cdot h[K - k] \tag{4}$$

The decomposition procedure starts by passing $f[k]$ through the HPF and LPF filters (level #1) and the obtained set of $cA[k]$ and $cD[k]$ coefficients is down-sampled by a factor of two as in (2), (3). Approximation coefficients can be further analysed at a next decomposition level, thus new approximation and detail coefficients are derived. Therefore, successive DWTs are performed until the desired resolution posed by the user is accomplished, as shown in the example of Fig. 1.

3. Proposed Methodology

The proposed measurement-based approach for the development of dynamic equivalent models is presented step-by-step in Fig. 2. Prior to parameter estimation, the method involves two pre-processing steps, namely event detection and signal de-noising. The overall procedure is automatic, facilitating the processing of the measured data and eventually the derivation of equivalent model parameters.

3.1. Event detection

Measured data of real power P, reactive power Q and voltage V are continuously recorded from measurement devices and processed within sliding windows $w_{v,k}$, with duration of 0.1 s, i.e., K' data points; k here denotes the time index of the last recorded sample included in the window. Note that, the selection of sliding windows of $w_{v,k} = 0.1$ s was guided by recommendations from the literature [13], as well as through extensive trial and error. The recording system may refer to conventional power quality (PQ) loggers or new class of measurement devices, such as micro-PMUs and PMUs. For the development of dynamic equivalent models, typically data related to obvious voltage disturbances are used [9]. The identification of the onset of the volage event, denoted for rest of the paper as t_0, is of crucial importance for the accurate estimation of the equivalent model parameters [13]. Therefore, in the framework of the proposed methodology, the voltage event onset is automatically identified via the following two-level procedure:

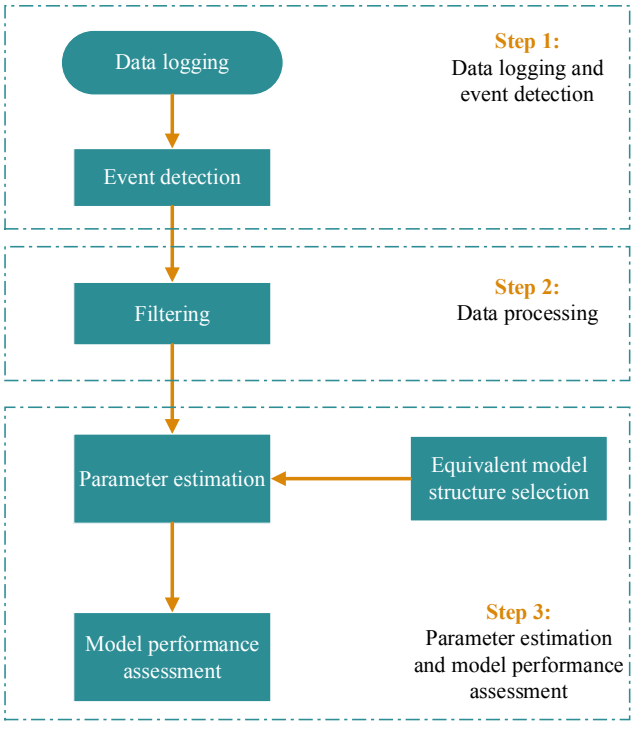

Figure 2: Flowchart of the proposed methodology.

- The relative difference RD of the signal energy, E_{k+1} and E_k, is calculated between two consecutive voltage sliding windows, $w_{v,(k+1)}$ and $w_{v,k}$, respectively as:

$$RD = \left| \frac{E_{k+1} - E_k}{E_{k+1}} \right| \cdot 100 \tag{5}$$

where $E_k = \sum_{k'=1}^{K'} \frac{w_{v,k}^2[k']}{K'}$. If RD is higher than a specific threshold, the disturbance detector is armed.

- If the disturbance detector is armed, the stationary DWT (SWT) is applied within $w_{v,(k+1)}$ and the calculated cD are used to identify t_0. SWT is a translation-invariance modification of the DWT, that does not decimate coefficients at every decomposition level. The wavelet-based method has been selected as one of the most widely used techniques for the automatic detection of abrupt changes in signals [11]. Note that, db1 mother wavelet (or Haar wavelet) is used due to its resemblance to the step up/down disturbance in the signals (see Fig. 3) [28]; a single-level structure is used to perform the signal SWT decomposition. Eventually, the event onset is set to t_0 by comparing the absolute value of cD, with a threshold. Commonly, fixed thresholds are used. Nevertheless, adaptive thresholding $\tilde{\delta}$ can ensure reliable and robust detection of events by taking into account the examined system conditions [29]. This way, the estimated cD are compared to [16]:

$$\tilde{\delta} = \delta_1 \cdot \text{mean}(cD) + \delta_2 \cdot \text{std}(cD) \tag{6}$$

where δ_1 and δ_2 are positive constants [30], determined via trial and error. In (6), the mean value (mean) represents the central tendency of the data set, and the standard deviation (std) its variability. Coefficients cD are calculated by analyzing the signal prior to the disturbance (ambient data). This way, $\tilde{\delta}$ can be adaptively determined for each system case.

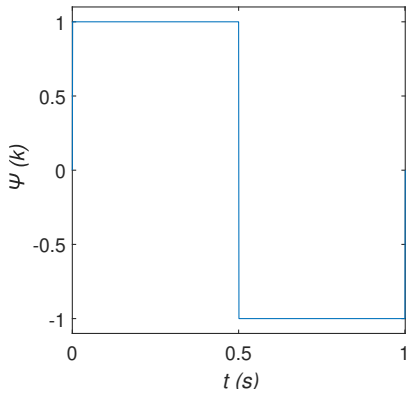

Figure 3: db1 (Haar) mother wavelet.

3.2. Filtering

Once the dynamic response has been captured, wavelet de-noising [31] is applied to remove noise and outliers to improve the Signal-to-Noise Ratio (SNR) of the measured signals and facilitate the parameter estimation procedure. Specifically, the DWT of the recorded signals is calculated and the resulting $cD[k]$ are compared to a specified threshold and processed, i.e, being completely or partially suppressed of some aspect of the signal. Next, the inverse DWT is applied to recover the original signal.

There are many methods to determine the filtering threshold. Among them, the universal threshold T_{UNIV}, described by (7), is the most widely used because of its simplicity and efficiency [32],

$$T_{UNIV} = \sigma \cdot \sqrt{2 \log K} \tag{7}$$

where σ is the signal standard deviation and K is the window length.

A different way to set the threshold is based on Stein's unbiased risk estimator (SURE), described by (8) [33], [34],

$$T_{SURE} = \sigma \cdot \sqrt{\omega_b} \tag{8}$$

where ω_b is the b-th coefficient wavelet square with the minimum risk [33], [35].

By combining the two approaches, this entails the Heuristic variant of Stein's unbiased risk estimate (HEURSURE). If SNR is low, the T_{UNIV} threshold is used; if SNR is high, the T_{SURE} threshold is applied [35]. In this study HEURSURE is used and the DWT coefficients are recalculated by means of soft thresholding [33]:

$$\begin{aligned} c_k^{'} &= \mathrm{sgn}(c_k) \cdot (c_k - T) \quad , \text{if } |c_k| \geqslant T \\ c_k^{'} &= 0 \qquad\qquad\qquad\quad , \text{if } |c_k| < T \end{aligned} \tag{9}$$

where T can be either T_{SURE} or T_{UNIV}, depending on the SNR. In this procedure, the level structure of the DWT is determined as $M = \log_2 K$ [36].

Finally, the parameter estimation is improved by focusing on the dynamic response dynamics; this necessitates to exclude non useful post-disturbance response data. Therefore, the optimal length of the analysis window is determined by applying the sliding window technique of [13].

3.3. Parameter Estimation and Modelling Evaluation

The recorded P, Q and V signals are used to identify the real and reactive power model parameters, θ_P and θ_Q, respectively, by applying an identification method to fit the input-output data. In particular, the model parameters are estimated via the nonlinear least square optimization technique [2], aiming to minimize (10),

$$J = \sum_{k=1}^{K} (y[k] - \hat{y}[k])^2 \tag{10}$$

where $y[k]$ is the response of the original signal (either P or Q) at the k-th sample and $\hat{y}[k]$ is the corresponding estimated response.

To evaluate the accuracy of the developed models the coefficient of determination index, R^2, is used:

$$R^2 = \left(1 - \frac{SSE}{SST}\right) \cdot 100. \tag{11}$$

where

$$SSE = \sum_{k=1}^{K} (y[k] - \hat{y}[k])^2 \tag{12}$$

$$SST = \sum_{k=1}^{K} (y[k] - \bar{y})^2 \tag{13}$$

Here, SSE is the sum of the squares of the vertical distances of the samples from the original data. SST is the sum of the squares of the vertical distances of the samples from a horizontal line drawn at $\bar{y}$, i.e., the mean value of the response $y[k]$.

R^2 is a measure of the goodness of fit. The more accurate the model prediction, the closer R^2 is to 100. Therefore, in the best case, where the modeled values exactly match the observed ones ($SSE = 0$), $R^2 = 100$. A baseline model, which always predicts $\bar{y}$ ($SSE = SST$) has $R^2 = 0$. Models that fit the data even worse than this baseline will present $SSE > SST$ and in turn $R^2 < 0$.

4. Noise Distributions

Real-world signals are most probably distorted due to measurement and ambient noise [26]. Gaussian (normal distribution) measurement error is typically assumed in power system testing [17]. However, results might be inaccurate if the Gaussian assumption is violated. Recent studies [17] on field measurements (amplitude and phase angle of voltage and current) have shown that for the realistic simulation of the measurement error non-Gaussian distributions with

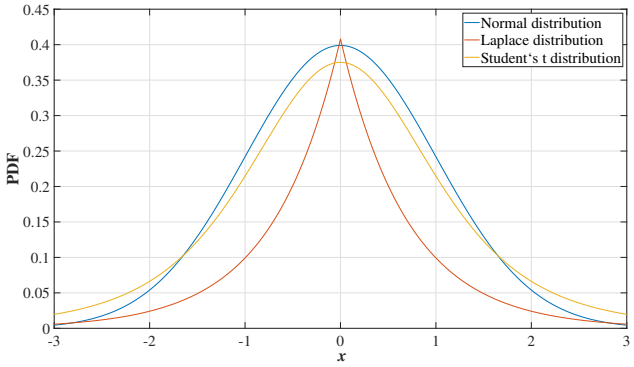

Figure 4: PDF of Gaussian, Laplace and Student's t distribution.

long tail should be considered. This type of distribution can be represented more accurately in terms of the Laplace or Student's-t distributions.

In Fig. 4 indicative probability density functions (PDF) of Gaussian, Laplace (also known as double exponential) and Student's-t distributions are compared to visualize their differences. The PDFs have been generated in the range [-3,3]. All distributions are bell-shaped symmetrical about their means and have been illustrated, assuming mean, $\mu = 0$, and standard deviation, $\sigma = 1.7323$. It can be seen that, the peak of the Laplace distribution is sharper than Gaussian and has a moderate tail, going to zero like the exponential function. Additionally, the Student's-t distribution includes an additional parameter, i.e., the degrees of freedom υ that controls the kurtosis of the PDF. Distributions with a small υ (more degrees of freedom) are taller and have thinner tails, presenting increased likelihood of outliers. In Fig. 4, $\upsilon = 4$; thus, the Student's-t distribution presents higher kurtosis than the Gaussian and consequently outliers are more likely to occur.

5. Evaluation Using Synthetic Signals

To evaluate the feasibility of the proposed framework in terms of accuracy of the simulated responses and model estimates, synthetic signals are used.

5.1. Synthetic Signal Generation

Two dynamic equivalents of different complexity are used to simulate real/reactive power dynamics subsequent to step voltage disturbances, i.e., the exponential recovery model (ERM) and the second-order recovery model (SORM). The ERM is extensively used to represent first-order dynamic responses [2] and is described by (14). The SORM is a second-order representation of the ERM capable to analyze more oscillatory responses, and it is described by (15).

$$y_e(t) = y_s(t) - (y_s(t) - y_t(t)) \cdot e^{-\frac{t-t_0}{T_y}}$$
$$y_s(t) = y_0 \cdot \left(\frac{V(t)}{V_0}\right)^{N_s} \quad y_t(t) = y_0 \cdot \left(\frac{V(t)}{V_0}\right)^{N_t} \tag{14}$$

Table 1
Real (θ_P) and reactive (θ_Q) power grid parameters

Grid type	Sets of model parameters
RCMs	$\boldsymbol{\theta_P} = \boldsymbol{\theta_{ERM}} = [0.1070, 1.0411, 0.2047]$ $\boldsymbol{\theta_Q} = \boldsymbol{\theta_{ERM}} = [1.4826, 1.9916, 0.1557]$
Small IMs	$\boldsymbol{\theta_P} = \boldsymbol{\theta_{SORM}} = [2100, 55, 2.5, 150]$ $\boldsymbol{\theta_Q} = \boldsymbol{\theta_{ERM}} = [0.3174, 4.9050, 0.0590]$

$$y_e(t) = \left(y_0 + \frac{b_0}{a_0}(V(t) - V_0)\right) + \left(e^{-\frac{a_1}{2}(t-t_0)}\right) \cdot \cdot \left[\frac{2a_0b_1 - a_1b_0}{2a_0\sqrt{a_0 - \frac{a_1^2}{4}}} \sin\left(\sqrt{a_0 - \frac{a_1^2}{4}}(t-t_0)\right) - \frac{b_0}{a_0}\cos\left(\sqrt{a_0 - \frac{a_1^2}{4}}(t-t_0)\right)\right](V(t) - V_0) \tag{15}$$

In (14) and (15), $y_e(t)$ is the simulated real/reactive power and $V(t)$ is the grid voltage. In addition, y_0 and V_0 are the power and voltage amplitude prior to the disturbance; t_0 is the time of disturbance. For real or reactive power modelling using the ERM, the $\boldsymbol{\theta_{ERM}} = [N_s,\ N_t,\ T_y]$ set of parameters must be identified [13]. For real or reactive power modelling using the SORM, the $\boldsymbol{\theta_{SORM}} = [a_0, a_1, b_0, b_1]$ parameter set must be identified [13].

The sets of model parameters used to generate the real and reactive power synthetic signals are presented in Table 1. These correspond to two distinct types of DNs: those dominated by residential-commercial motors (RCMs) and by small IMs [13]. Note that the synthetic signals are generated by applying step-down voltage disturbances at $t_0 = 0.5$ s, that are equal to either - 1.25% or - 2.50%; a sampling rate of 1000 samples per second (sps) is assumed.

5.2. Distorted Dynamic Responses

In Fig. 5, real and reactive power responses of DNs dominated by RCM are presented for the two voltage step-down disturbances. The pure synthetic signals, i.e., voltage amplitude and real and reactive power are distorted by additive noise in terms of Gaussian, Laplace and Student's t distribution to replicate realistic conditions. Originally, these distributions concern the quantities monitored directly by the measurement devices, i.e., amplitude and phase angle of measured voltage and current. In turn, it is assumed that also the resulting calculated quantities, i.e., real and reactive power are distorted following a similar distribution. The SNR is 20 dB [37]. The corresponding responses for DNs dominated by small IMs are plotted in Fig. 6.

For both models, it can be seen that the voltage step causes a power response that can be described by two phases. In the first phase (transient part), a step in real and reactive power follows immediately the abrupt voltage change; thus,

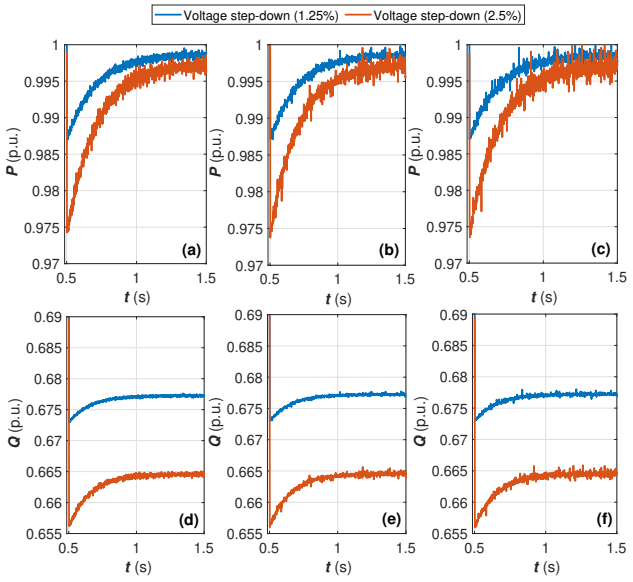

Figure 5: RCM real power response distorted by (a) Gaussian, (b) Laplace and (c) Student's-t noise distribution. RCM reactive power distorted by (d) Gaussian, (e) Laplace and (f) Student's-t noise distribution.

the equivalent DN model during this phase behaves as an impedance and represents the invariable IM slip during the voltage step [38]. The undershoot for the RCM real and reactive power response is for the -1.25%/-2.5% voltage disturbances 1.6%/2.6% and 2.5%/4.9%, respectively. The corresponding values for the small IM case are 2.0%/4.2% and 5.8%/10.9%. It can be realized that the reactive power response is more sensitive to the level of disturbance for

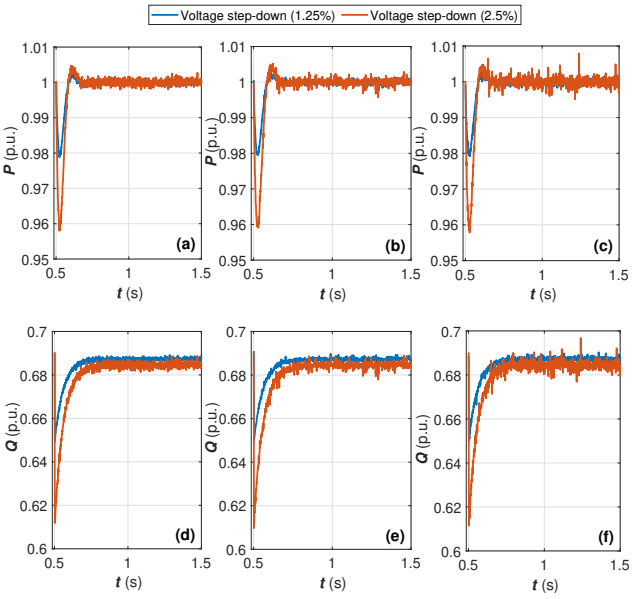

Figure 6: Small IM real power response distorted by (a) Gaussian, (b) Laplace and (c) Student's-t noise distribution. Small IM reactive power distorted by (d) Gaussian, (e) Laplace and (f) Student's-t noise distribution.

both models. Moreover, the impact of parameter N_t on power dynamics can be easily understood by comparing the overshoots of reactive power for the RCM and small IM case. Indeed, the higher the value of N_t, the bigger the overshoot. In the second phase (recovery part) a new steady-state is gradually established. The dynamics of the DN tend to restore the grid power to a certain extent. With respect to (14), the reactive power (for both models) and the RCM real power recover almost in exponential form; on the other hand for the small IM real power the recovery is more oscillatory (see (15)), presenting a peak at around 0.6 s. Note that, the undershoot and the new steady-state are related non-linearly to the voltage response [38]. In fact, the real power for both models recovers almost to the same value prior to the disturbance. However, this is not the case for the reactive power, where the new steady-state values differ significantly compared to the pre-disturbance ones, as the voltage disturbance level increases. The observed differences dependent on N_s values. The difference is more pronounced for the RCM model as $N_s = 1.4826$, and thus considerably higher compared to the IM case. In fact, for the RCM case the difference in the steady-state prior to and after to the disturbance is equal to 1.84%.

Considering the influence of noise distribution, responses distorted by Gaussian noise present generally a smooth shape. On the other hand, as expected, under the Laplace distribution and more importantly under the Student's-t, outliers, i.e., excessive spikes, at different time instants are observed.

5.3. Event Detection Procedure Assessment

The performance of the proposed event detection method is evaluated considering the Student's-t noise distribution to simulate measurement error in a realistic way and include also outliers. The noisy voltage response and the corresponding SWT cD are presented in Fig. 7 for the two step-down disturbances, assuming SNR=20 dB. In the figure, the red asterisk points the onset of the disturbance, detected by the proposed method. In addition, the value of the adaptive

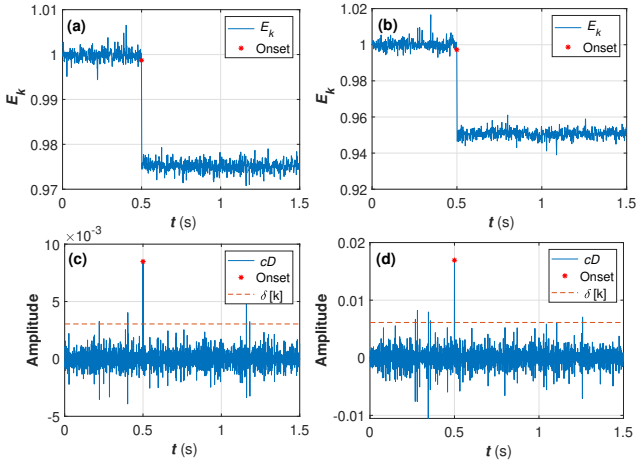

Figure 7: Calculated a) E_k, c) cD for 1.25% disturbance, and b) E_k, d) cD, for 2.5% disturbance.

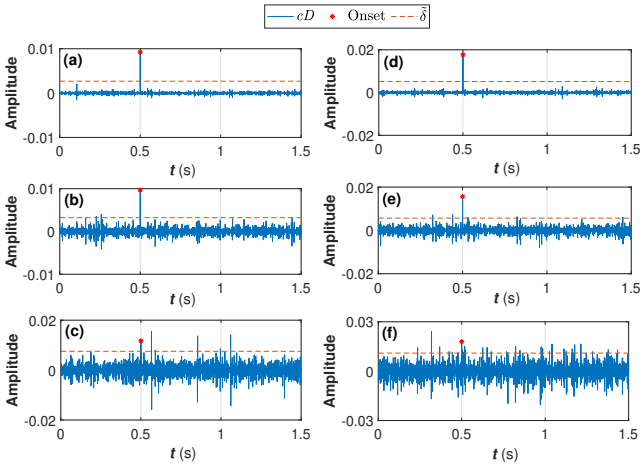

Figure 8: cD for 1.25% disturbance, a) 30 dB, b) 20 dB and c) 10 dB, and for 2.5 %, d) 30 dB, e) 20 dB and f) 10 dB.

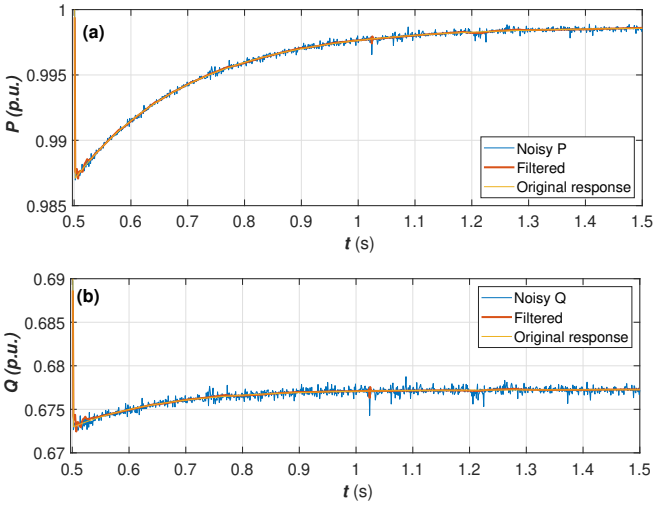

Figure 9: Responses of the a) real and b) reactive power, distorted by Student's t noise for SNR = 20 dB, filtered with WT.

threshold that sets the start of the event is plotted with a dashed line. After exhaustive trial and error trials RD is set to 2.5% and the parameters of the adaptive thresholding are $\delta_1 = 0.4$ and $\delta_2 = 2$. It is evident that the value of the threshold $\tilde{\delta}$ differs per case as depends on the system conditions. Results verify that the voltage event is successfully identified in all cases.

To investigate the performance of the proposed event-detection technique under different noise environments, the voltage response is distorted with adjusted variance noise to replicate SNR levels of 10 dB, 20 dB and 30 dB [39]. In Fig. 8 the calculated cD is plotted with respect to the adaptive threshold and the detected time of disturbance. The excessive spikes in the signal and consequently in the cD may result into false event triggering. This is more pronounced with decreasing SNR. However, this is avoided, as the selected RD threshold is not exceeded; thus, RD thresholding is used as a complementary technique to filter out signal outliers.

5.4. Filtering

The efficiency of the proposed DWT-based denoising method is evaluated and compared with the LPF, the MA and SG [13], [40]. Optimum filter design parameters have been selected after exhaustive trial and error. In particular, for DWT-based denoising db1 and db2 mother wavelets have been used for the voltage and real/reactive power responses, respectively [28]; a 10^{th} order LPF is used with cutoff frequency equal to 21 Hz, a MA filter with frame length 10 samples and a 10^{th} order SG filter with frame length equal to 25 samples [13]. The performance of the filtering techniques is evaluated in terms of R^2, assuming that in (11) the estimated response, $\hat{y}[n]$, has been calculated as follows: i) apply filtering to the distorted response, ii) estimate the model parameters via (10) and iii) simulate the real and reactive model responses via (14) or (15) by using the identified model parameters. Real and reactive power signals are generated and distorted in terms of the three noise distributions for SNR levels 10 dB, 20 dB and 30 dB. For each case 100 Monte Carlo (MC) simulations are conducted; a random instance by applying DWT-based denoising considering Student's-t noise distribution and SNR = 20 dB is

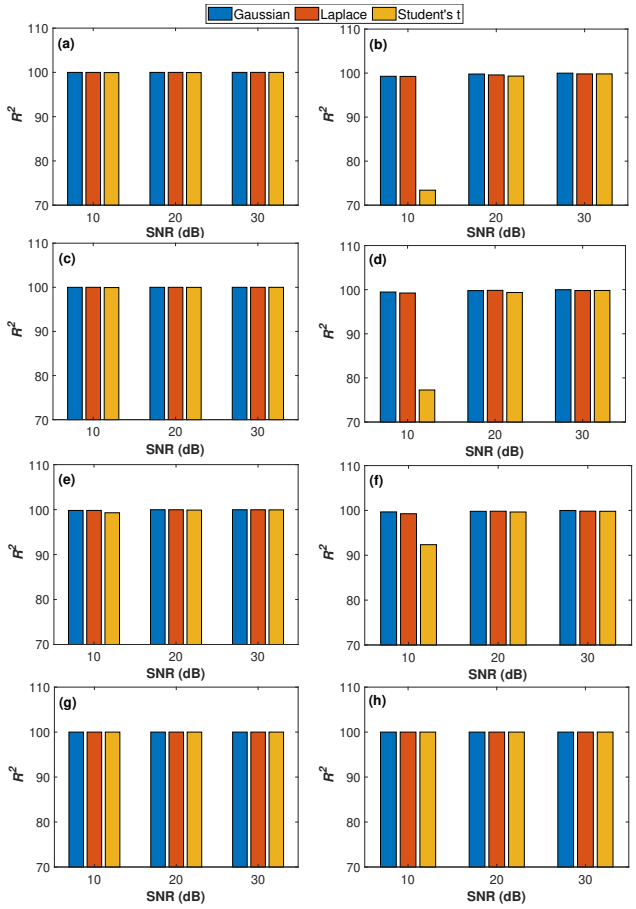

Figure 10: R^2 of LPF for a) real power, b) reactive power, of MA for c) real power, d) reactive power, of SG for e) real power, f) reactive power, and of WT for g) real power and h) reactive power.

depicted in Fig. 9 for the RCM model. The optimal length of the analysis window is approximately 1s.

In Fig. 10 the calculated R^2 is summarized for the different filtering methods. Results are analysed per SNR level by plotting the mean R^2 of the MC corresponding simulations. Note that, to ensure consistency in the comparisons, outlier R^2 estimates have been identified with the aid of box plots [40] and removed. In fact, this is the case for SNR = 10 dB, where 10 cases (on average) were considered as outliers and were eventually removed for the analysis of the LPF, MA and SG results; for the DWT-based denoising no outliers have been identified. It is evident that high real power R^2 values are obtained for all filtering techniques and noise cases. Therefore, the distinct dynamic features of the response have been preserved. Similar remarks can be also deduced considering the reactive power response when the pure signal is distorted by Gaussian and Laplace noise. However, this is not the case for SNR = 10 dB Students'-t noise distribution. Indeed, significant performance degradation is observed for the LPF, MA and SG filtering techniques. On the other hand, the DWT-based de-noising outperforms these techniques regarding noise and outliers removal as it preserves its high accuracy. For the small IM scenario the resulting R^2 is close to 100% for all cases; thus, the corresponding bar graphs are not presented. Therefore, by comparing the two DN cases, it can be deduced that the modelling of the RCM reactive power response is more challenging than the rest dynamic responses, i.e., RCM real power and small IM real/reactive power, due to its distinct dynamic characteristics. To better elaborate on this, let us assume for example the N_s parameters of the RCM and the small IM DN models. It can be realized that the RCM reactive power pertains to a response with significant difference between the steady-state values prior to and after the disturbance; thus being more vulnerable to the effect of noise and outliers.

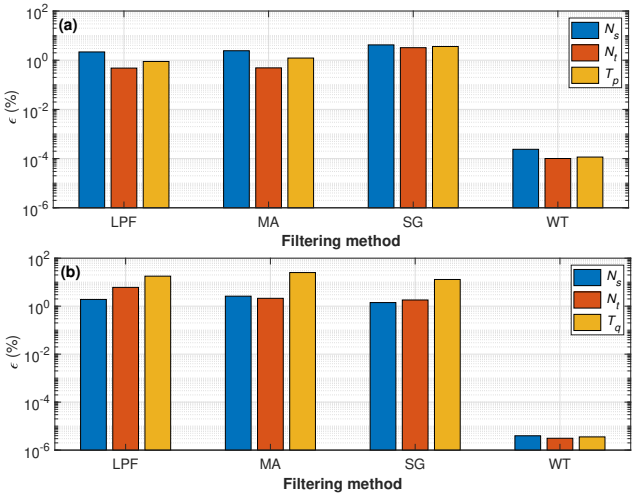

Figure 11: Parameter percentage error by using the four filtering methods for the DN dominated by RCM for the a) real power and b) reactive power. Student's-t noise with SNR = 10 dB.

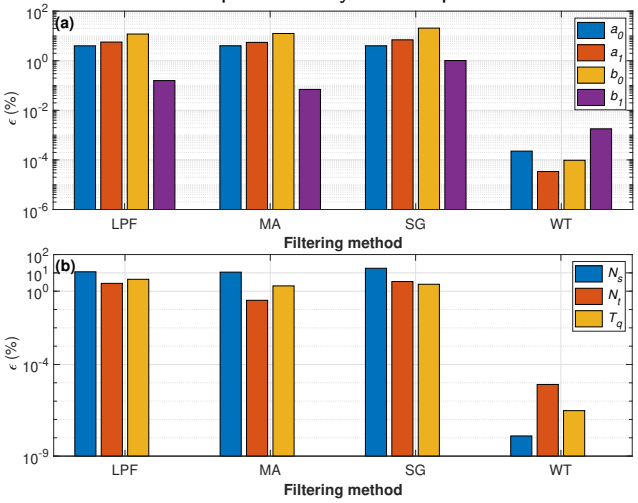

Figure 12: Parameter percentage error by using the four filtering methods for the DN dominated by small IM for the a) real power and b) reactive power. Student's-t noise with SNR = 10 dB.

Additionally, the efficiency of the examined filtering techniques is evaluated in terms of model parameter estimates. The % error (ϵ) is calculated by comparing the average value of the model parameters derived from the 100 MCs, to the original ones. Indicatively, the case of Students'-t distribution and SNR = 10 dB is depicted in Figs. 11 and 12 for the RCM and the small IM models. It is shown that the parameters derived by applying the proposed WT-based methodology are almost identical to the original. On the other hand, deviations are observed for the LPF, MA and SG techniques. These become more marked considering the reactive power responses.

6. Simulation Study in a Large-Scale Distribution Network

The scalability of the WT-based method is tested in a large-scale MV simulation model, illustrated in Fig. 13. The test system used is a modified version of the CIGRE benchmark European MV distribution grid [41]. The applied modifications are summarised as follows [42]: i) only the first feeder is used in the model, ii) switches are open, and iii) the total system load (4590 kVA) is evenly distributed among the DN buses.

Two network operating scenarios are being studied, i.e., conventional DN and ADN. In the former, network end-users are exclusively loads, comprising of static and dynamic components. The static loads are represented as constant impedance loads and the dynamic loads are characterized using Type-7 IM model parameters [43]. In the ADN scenario, the examined DN is further modified by adding DRES units uniformly across all system buses. DRES are simulated using the Type 4A model [44]. The Type 4A model is a generic representation/model of full-scale converter-interfaced generation units, such as wind generators and photovoltaics. For the purpose of the analysis, DRES operate under the constant power (P-Q) mode. In total, four test cases are studied by varying the dynamic load participation in the

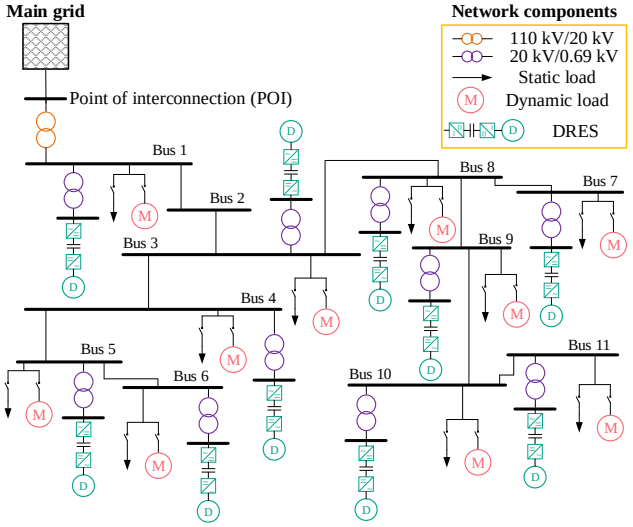

Figure 13: Examined MV simulation model.

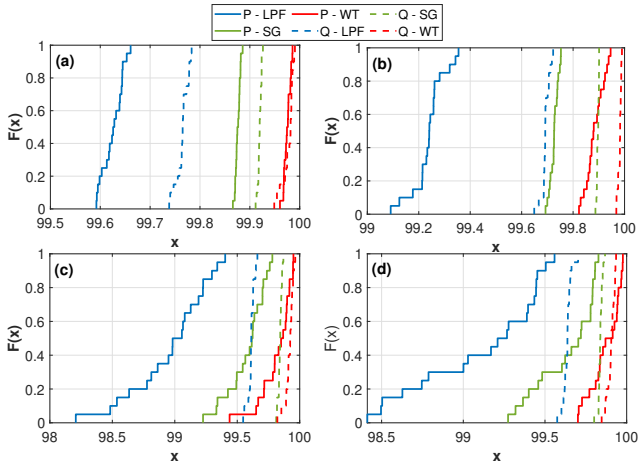

Figure 14: Comparison of the filtering methods by means of CDFs. a) Case #1, b) Case #2, c) Case #3, and d) Case #4.

total load mix, as well as the DRES penetration level (with respect to the total system load power), namely:

- Case #1 (**conventional DN**): 40% static load, 60% dynamic load, 0% DRES penetration.
- Case #2 (**conventional DN**): 0% static load, 100% dynamic load, 0% DRES penetration.
- Case #3 (**ADN**): 40% static load, 60% dynamic load, 20% DRES penetration.
- Case #4 (**ADN**): 40% static load, 60% dynamic load, 40% DRES penetration.

Since the dynamic performance of the distribution network is considerably influenced by the pre-disturbance voltage level at the point of interconnection (POI) with the transmission network, the examined test cases consider three distinct operating conditions ranging from 0.95 to 1.05 p.u. For each test case, a total of $N_D = 20$ step-down and step-up disturbances ranging from -0.1 p.u. to 0.1 p.u. are induced by tap changing on the secondary side of the 110kV/20kV transformer. The dynamic responses of voltage, real and reactive power are obtained at POI. The responses are generated at 1000 sps and subsequently are distorted by random noise with Student's-t PDF for SNR = 20 dB. The proposed WT-based method ($RD = 2.5\%$, $\delta_1 = 0.4$ and $\delta_2 = |3|$; absolute value is used for both step-up and step-down disturbances) is applied to capture the dynamic responses and filter out noise and outliers. Further details on the DRES siting and sizing are provided in [42]. The above cases are simulated in PowerFactory - DIgSILENT software [21].

The performance of WT denoising is evaluated by analysing the R^2 cumulative distribution function (CDF) of $N_D = 20$ discrete simulations in Fig. 14 for the four different test cases. Note that, R^2 has been calculated under the same premises of Section 5, considering an optimal window length (per test case) for the post-processing analysis [13]. In addition, in the same figure, the CDF plots for the LPF and the SG filtering techniques are provided. The MA method has been also examined, however, the obtained results show significantly lower R^2 values, thus have not been presented. For the LPF, MA and SG filters the same parameters as for the synthetic signals apply. Comparisons indicate that the proposed WT-based method presents in all cases the highest R^2 value (over 99.5%) for both the real and reactive power signals. Comparable, although lower R^2 results, are also obtained for the rest of the examined filtering techniques, especially for the SG method. It can be also noticed that signal filtering becomes slightly more challenging as the dynamic load and DRES penetration increases since generally lower R^2 values are obtained; this is more marked for the real power response.

7. Application to Measurements

The applicability of the proposed method is also tested in analyzing measured responses. These have been recorded at the POI of a low-voltage laboratory-scale microgrid (MG) [45]. As shown in Fig. 15, a three-phase programmable voltage source (PVS) supplies the test setup.

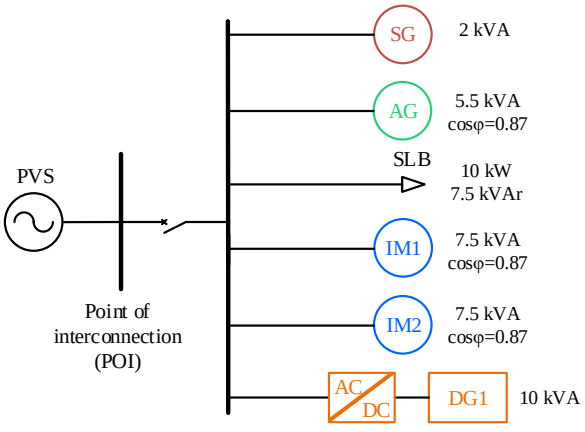

Figure 15: Laboratory-scale MG.

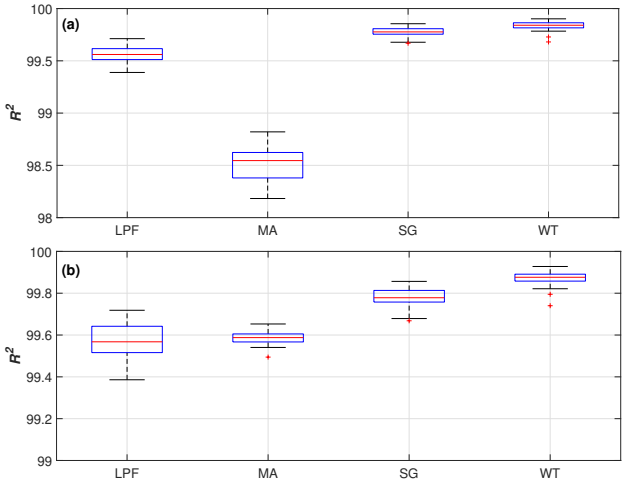

Figure 16: Comparison of filtering methods considering a) real power responses, and b) reactive power responses.

One synchronous (SG), one asynchronous (AG) and one inverter interfaced unit (DG1) constitute the generation of the MG; the load demand comprises a static load bank (SLB) and two asynchronous motors (IM1 & IM2). A set of 30 dynamic responses (V, P, Q) are recorded at 500 sps by applying step-voltage disturbances in the range of -0.1 p.u. to 0.1 p.u. at the MG point of interconnection. The optimal window length has been determined to 2.3 s [13].

The performance of the four filtering techniques is compared in Fig. 16 by means of boxplots. More specifically, results for real and reactive power are presented in Fig. 16a and 16b, respectively. For the LPF, MA and SG filters the same parameters as in the preceding cases have been used and for the WT-based method, $RD = 6\%$, $\delta_1 = 0.4$ and $\delta_2 = |2|$. With this test the efficiency of the WT-based method is substantiated also with measured data, as the highest R^2 (over 99.5%) is calculated. Moreover, results verify that SG and LPF can be also reliable tools for the filtering of dynamic responses in power systems. The average computational burden of the entire process, excluding parameter estimation, remains under 0.4 seconds; computations were conducted utilizing a PC equipped with an i7-8550U processor running at 1.8 GHz, with 8 GB of RAM.

8. Discussion and Conclusions

This paper presents an analytical study of processing measured dynamic responses by using the DWT. Such measurements can be obtained at indicative substations of DNs during voltage disturbances. The proposed method has been evaluated using synthetic signals, RMS simulated responses and laboratory measurements.

In the case of pure signals, in order to replicate real world conditions, the responses have been distorted considering different types of noise distribution. More explicitly, the widely adopted Gaussian noise as well as distributions with long tail, i.e., Laplace and Student's-t that represent more realistically the measurement error have been applied.

The conducted analysis has shown that the proposed two-level event detection procedure can automatically identify the exact time of the disturbance onset even under severe noise conditions with outliers. A failure to identify the onset of a disturbance entails significant errors in the derivation of the model parameters.

The LPF, MA, SG and WT-based filtering techniques can efficiently filter out distorted signals. The WT-based filtering generally presents more smooth responses and accurate mode estimates compared to the rest techniques. This becomes more marked in highly noisy environments assuming the Laplace and Students'-t noise distributions. In fact, in such extreme cases only the proposed WT-based technique can improve significantly the quality of the signal and lead to the derivation of accurate model parameters.

In essence, the proposed method constitutes a reliable overall signal analysis method that can be efficiently used to enhance the quality of the distorted signals and further be applied to investigate the dynamic behavior of DNs.

Evaluation with field measurements of dynamic responses and ambient data obtained at the POI of DNs would certainly contribute to the further enhancement of the proposed methodology and the development of dynamic equivalent models of DNs for different operating conditions.

CRediT authorship contribution statement

Efthimios P. Saroudis: Investigation, Formal Analysis, Methodology, Writing - Original draft preparation. **Theofilos A. Papadopoulos:** Conceptualization of this study, Writing - Original draft preparation, Supervision. **Georgios A. Barzegkar-Ntovom:** Data curation, Validation, Writing - Original draft preparation. **Eleftherios O. Kontis:** Data curation, Validation, Writing - Original draft preparation. **Nikolaos Mitianoudis:** Writing - Review & Editing. **Grigoris K. Papagiannis:** Writing - Review & Editing.

References

[1] Y. Zeng, D. Meng, B. Liu, X. Hu, and W. Luan, "Load component decomposition and online modelling based on small disturbance response characteristic matching," *IET Gener. Transm. Distrib.*, vol. 16, 11 2021.

[2] CIGRE Task Force, *Modelling and Aggregation of Loads in Flexible Power Networks*. CIGRE Working Group C4.605, Paris, France, Tech. Rep. 566, 2014.

[3] I. D. Pasiopoulou, E. O. Kontis, T. A. Papadopoulos, and G. K. Papagiannis, "Effect of load modeling on power system stability studies," *Electr. Power Syst. Res.*, vol. 207, 2022.

[4] G. Chaspierre, G. Denis, P. Panciatici, and T. Van Cutsem, "An active distribution network equivalent derived from large-disturbance simulations with uncertainty," *IEEE Trans. Smart Grid*, vol. 11, no. 6, pp. 4749–4759, 2020.

[5] N. Fulgencio, C. Moreira, L. Carvalho, and J. P. Lopes, "Aggregated dynamic model of active distribution networks for large voltage disturbances," *Electr. Power Syst. Res.*, vol. 178, 2020.

[6] E. O. Kontis, T. A. Papadopoulos, A. I. Chrysochos, and G. K. Papagiannis, "Measurement-based dynamic load modeling using the

vector fitting technique," *IEEE Trans. Power Syst.*, vol. 33, no. 1, pp. 338–351, 2017.

[7] G. Mitrentsis and H. Lens, "Data-driven dynamic models of active distribution networks using unsupervised learning techniques on field measurements," *IEEE Trans. Smart Grid*, vol. 12, no. 4, pp. 2952–2965, 2021.

[8] B.-K. Choi, H.-D. Chiang, Y. Li, H. Li, Y.-T. Chen, D.-H. Huang, and M. Lauby, "Measurement-based dynamic load models: derivation, comparison, and validation," *IEEE Trans. Power Syst.*, vol. 21, no. 3, pp. 1276–1283, 2006.

[9] Y. Zhu and J. V. Milanović, "Automatic identification of power system load models based on field measurements," *IEEE Trans. Power Syst.*, vol. 33, no. 3, pp. 3162–3171, 2018.

[10] C. Wang, Z. Wang, J. Wang, and D. Zhao, "SVM-Based Parameter Identification for Composite ZIP and Electronic Load Modeling," *IEEE Trans. Power Syst.*, vol. 34, no. 1, pp. 182–193, 2019.

[11] D.-I. Kim, T. Y. Chun, S.-H. Yoon, G. Lee, and Y.-J. Shin, "Wavelet-based event detection method using PMU data," *IEEE Trans. Smart Grid*, vol. 8, no. 3, pp. 1154–1162, 2017.

[12] T. A. Papadopoulos, E. O. Kontis, G. A. Barzegkar-Ntovom, and P. N. Papadopoulos, "A three-level distributed architecture for the real-time monitoring of modern power systems," *IEEE Access*, vol. 10, pp. 29 287–29 306, 2022.

[13] G. A. Barzegkar-Ntovom, T. A. Papadopoulos, and E. O. Kontis, "Robust framework for online parameter estimation of dynamic equivalent models using measurements," *IEEE Trans. Power Syst.*, vol. 36, no. 3, pp. 2380–2389, 2021.

[14] K. N. Hasan, J. V. Milanović, P. Turner, and V. Turnham, "A step-by-step data processing guideline for load model development based on field measurements," in *2015 IEEE Eindhoven PowerTech*, 2015, pp. 1–6.

[15] N. Zhou, P. John, D. Trudnowski, and R. Guttromson, "Robust RLS methods for online estimation of power system electromechanical modes," *IEEE Trans. Power Syst.*, vol. 22, no. 3, pp. 1240–1249, 2007.

[16] N. Zhou, Z. Huang, F. Tuffner, J. Pierre, and S. Jin, "Automatic implementation of prony analysis for electromechanical mode identification from phasor measurements," *IEEE PES General Meeting*, pp. 1–8, 2010.

[17] S. Wang, J. Zhao, Z. Huang, and R. Diao, "Assessing Gaussian Assumption of PMU Measurement Error Using Field Data," *IEEE Trans. Power Deliv.*, vol. 33, no. 6, pp. 3233–6, 2018.

[18] D. Trudnowski and J. Piere, "Signal processing methods for estimating small-signal dynamic properties from measured responses" in inter-area oscillations in power systems: A nonlinear and nonstationary perspective," *Boston, MA, USA: Springer*, 2009.

[19] A. Arif, Z. Wang, J. Wang, B. Mather, H. Bashualdo, and D. Zhao, "Load modeling—a review," *IEEE Trans. Smart Grid*, vol. 9, no. 6, pp. 5986–5999, 2018.

[20] E. P. Saroudis, T. A. Papadopoulos, G. A. Barzegkar-Ntovom, E. O. Kontis, and G. K. Papagiannis, "Wavelet-based automatic processing of dynamic responses for the development of dynamic load models," in *2022 2nd International Conference on Energy Transition in the Mediterranean Area (SyNERGY MED)*, 2022, pp. 1–6.

[21] DIgSILENT GmbH, "DIgSILENT Solutions PowerFactory Version 20."

[22] H. Guo, K. Rudion, H. Abildgaard, P. Komarnicki, and Z. A. Styczynski, "Parameter estimation of dynamic load model using field measurement data performed by OLTC operation," *IEEE Power and Energy Society General Meeting*, pp. 1–7, 2012.

[23] X. Zhu and B. Mather, "DWT-based aggregated load modeling and evaluation for quasi-static time-series simulation on distribution feeders," *IEEE PES GM*, pp. 1–5, 2018.

[24] G. Strang and V. Strela, "Orthogonal multiwavelets with vanishing moments," *Opt. Eng.*, vol. 33, no. 7, pp. 2104–7, 1994.

[25] A. Graps, "An introduction to wavelets," *IEEE Computational Science and Engineering*, vol. 2, no. 2, pp. 50–61, 1995.

[26] T. Edwards, "Discrete wavelet transforms: Theory and implementation," pp. 28–35, 1991.

[27] S. Avdakovic, A. Nuhanovic, M. Kusljugic, and M. Music, "Wavelet transform applications in power system dynamics," *Electr. Power Syst. Res.*, vol. 83, no. 1, pp. 237–245, 2012.

[28] W. K. Ngui, M. S. Leong, L. M. Hee, and A. M. Abdelrhman, "Wavelet analysis: Mother wavelet selection methods," *Appl. Mech. Mater.*, vol. 393, pp. 953 – 8, 2013.

[29] C. Longo, T. Burr, and K. Myers, "Change detection using wavelets in solution monitoring data for nuclear safeguards," *Axioms*, vol. 2, no. 2, pp. 271–285, 2013.

[30] J. Bello, L. Daudet, S. Abdallah, C. Duxbury, M. Davies, and M. Sandler, "A tutorial on onset detection in music signals," *IEEE Transactions on Speech and Audio Processing*, vol. 13, no. 5, pp. 1035–1047, 2005.

[31] D. L. Donoho, "Nonlinear wavelet methods for recovery of signals, densities, and spectra from indirect and noisy data," in *Proceedings of Symposia in Applied Mathematics*. American Mathematical Society, 1993, pp. 173–205.

[32] D. L. Donoho and I. M. Johnstone, "Ideal spatial adaptation by wavelet shrinkage," *Biometrika*, vol. 81, pp. 425–455, 1994.

[33] D. Valencia, D. Orejuela, J. Salazar, and J. Valencia, "Comparison analysis between rigrsure, sqtwolog, heursure and minimaxi techniques using hard and soft thresholding methods," *XXI Symposium on Signal Processing, Images and Artificial Vision*, pp. 1–5, 2016.

[34] C. M. Stein, "Estimation of the Mean of a Multivariate Normal Distribution," *Ann. Statist.*, vol. 9, no. 6, pp. 1135–1151, 1981.

[35] N. Verma and A. Verma, "Performance analysis of wavelet thresholding methods in denoising of audio signals of some indian musical instruments," *Int. J. Eng. Sci. Technol*, vol. 4, no. 5, pp. 2040–5, 2012.

[36] M. Yang, Y.-F. Sang, C. Liu, and Z. Wang, "Discussion on the choice of decomposition level for wavelet based hydrological time series modeling," *Water*, vol. 8, no. 5, 2016.

[37] J. K. Hwang and Y. Liu, "Noise analysis of power system frequency estimated from angle difference of discrete fourier transform coefficient," *IEEE Trans. Power Deliv.*, vol. 29, no. 4, pp. 1533–1541, 2014.

[38] D. Karlsson and D. Hill, "Modelling and identification of nonlinear dynamic loads in power systems," *IEEE Trans. Power Syst.*, vol. 9, no. 1, pp. 157–166, 1994.

[39] "IEEE task force on identification of electromechanical modes, identification of electromechanical modes in power systems." *IEEE Power & Energy Society, PES-TR15*, 2012.

[40] T. A. Papadopoulos, G. A. Barzegkar-Ntovom, V. C. Nikolaidis, P. N. Papadopoulos, and G. M. Burt, "Online parameter identification and generic modeling derivation of a dynamic load model in distribution grids," in *2017 IEEE Manchester PowerTech*, 2017, pp. 1–6.

[41] CIGRE, "Benchmark systems for network integration of renewable and distributed energy resources," *CIGRE Task Force C6.04.02*, 2014.

[42] G. A. Barzegkar-Ntovom, E. O. Kontis, T. A. Papadopoulos, and P. N. Papadopoulos, "Methodology for Evaluating Equivalent Models for the Dynamic Analysis of Power Systems," *IEEE Trans. Power Del.*, vol. 37, no. 6, pp. 5059–5070, 2022.

[43] "Standard load models for power flow and dynamic performance simulation," *IEEE Trans. Power Syst.*, vol. 10, no. 3, pp. 1302–1313, 1995.

[44] "Electrical Simulation Models – Generic Models," *IEC Wind Energy Generation Systems Part 27-1*, 2020.

[45] E. O. Kontis, T. A. Papadopoulos, M. H. Syed, E. Guillo-Sansano, G. M. Burt, and G. K. Papagiannis, "Artificial-Intelligence Method for the Derivation of Generic Aggregated Dynamic Equivalent Models," *IEEE Trans. Power Syst.*, vol. 34, no. 4, pp. 2947–2956, 2019.